Structural Evolution of Poly(styrene-*b*-4-vinylpyridine) Diblock Copolymer/Gold Nanoparticle Mixtures from Solution to Solid State

Ching-Mao Huang and Kung-Hwa Wei*

Department of Materials Science and Engineering, National Chiao Tung University, Hsinchu, Taiwan 30049, ROC

U-Ser Jeng and Keng S. Liang

National Synchrotron Radiation Research Center, 101 Hsin-Ann Road, Science-Based Industrial Park, Hsinchu, Taiwan 30077, ROC

Received February 25, 2007; Revised Manuscript Received May 10, 2007

ABSTRACT: We used in situ annealing small-angle X-ray scattering to monitor the structural evolution of a spherical poly(styrene-*b*-4-vinylpyridine) diblock copolymer (PS-*b*-P4VP)/2-phenylethanethiol-coated Au nanoparticle ($AuSC_2Ph$) mixture in the solid state during its thermal annealing. We found that the Au nanoparticles (NPs) that existed initially in a random state with some cluster packing in the PS domain diffused to the interface of the amphiphilic PS-*b*-P4VP diblock copolymer within 4 h at 170 °C under vacuum to form NP-filled shell-like assemblies, as further evidenced from transmission electron microscopy imaging. From the X-ray photoelectron spectroscopy data, we speculate that this interfacial activity of $AuSC_2Ph$ results from the fact that the initially hydrophobic Au NP surfaces became increasingly hydrophilic as most of the 2-phenylethanethiol ligands had evaporated off. The Au NP nanoshell assemblies located at the interface between PS and P4VP were quite stable even after redissolving in toluene; they remained in the form of PS−Au−P4VP core/shell/corona onion micelles, as evidenced from solution state small-angle X-ray scattering data.

Introduction

Diblock copolymer/nanoparticle (NP) mixtures have attracted much attention recently because their dimensions are comparable; for example, diblock copolymers can have ordered structures with periodic thicknesses between 10 and 100 nm, while NPs having sizes between 1 and 10 nm have the most interesting optical, electrical, and magnetic properties.[1−5] Hence, using diblock copolymers as templates to control the spatial positions of NPs is a natural approach to producing hierarchically ordered structures for various applications.[5−14] In this regard, the location of NPs in block copolymers, which critically affects their resulting properties, has been the focus of a number of theoretical and experimental studies.[15−28] For instance, Balazs et al. used self-consistent-field and density functional theories to predict the locations of NPs; they found that NPs can reside either along the interface of two blocks or in the center of one particular block, depending on the ratio of the size of the NPs to the periodic thickness of the diblock copolymer.[18−22] Nevertheless, only a few experimental studies have confirmed Balazs' prediction.[6b,10,17,23−28] To gain a fundamental understanding of the structures of the diblock copolymer/NP mixtures, we monitored the structural evolution of a particular system—poly(styrene-*b*-4-vinylpyridine)/gold NP (PS-*b*-P4VP/Au) assemblies—from solution to the solid state to the solid state experiencing annealing.

In this present study, we used small-angle X-ray scattering to follow the diffusion of hydrophobic gold NPs from continuous hydrophobic PS domains to the interfaces between the hydrophilic P4VP and hydrophobic PS. We also analyzed the hierarchical NP-filled shell structures that resulted from thermal annealing under vacuum. The structures of the redissolved PS-*b*-$P4VP_{Sph}$/Au NP systems that had experienced annealing in the bulk were also examined.

* To whom correspondence should be addressed: Tel 886-35-731871, Fax 886-35-724727, e-mail khwei@cc.nctu.edu.tw.

Experimental Section

Materials. The spherical PS-*b*-P4VP diblock copolymer (volume fraction of P4VP domain: 0.12), having a molecular weight (M_n) of 557KPS/75KP4VP with a polydispersity index (M_w/M_n) of 1.07, was purchased from Polymer Source, Inc. Hydrogen tetrachloroaurate(III) trihydrate ($HAuCl_4 \cdot 3H_2O$), tri-*n*-octylammonium bromide (TOAB, 99%), and sodium borohydride ($NaBH_4$, 99%) were obtained from Acros. 2-Phenylethanethiol (HSC_2Ph, 98%) was purchased from Aldrich. Toluene (99%), acetone (99%), dichloromethane (99%), and ethanol (99%) were purchased from TEDIA. Ultrapure deionized water was produced using a DirectQ3 system equipped with a pump from Millipore, Inc.

Synthesis of 2-Phenylethanethiolate-Coated and Pyridine-Coated Au NPs. 2-Phenylethanethiolate-coated Au NPs ($AuSC_2Ph$) were synthesized using the two-phase method described by Brust et al.[29,30] A typical procedure for producing the $AuSC_2Ph$ NPs is described as follows: An aqueous solution (3 mL) of $HAuCl_4$ (100 mg, 0.24 mmol) was mixed with a solution of tri-*n*-octylammonium bromide (332 mg, 0.60 mmol) in toluene (12 mL). The mixture was vigorously stirred until all of the $HAuCl_4$ had transferred into the organic layer. The organic phase was isolated when it had become dark brown in color. Subsequently, 2-phenylethanethiol (68 μL, 0.48 mmol) was added to the organic phase; after stirring for 20 min, the solution became colorless for a while. Next, a freshly prepared chilled aqueous solution (10 mL) of sodium borohydride (91 mg, 2.4 mmol) was added slowly with vigorous stirring over 30 min. Finally, after stirring for a further 24 h, the organic phase was separated, concentrated (rotary evaporator) to a volume of 1 mL, and then washed three times with ethanol and acetone to remove any excess thiol or other agents. Before dissolving in toluene, the sample was dried under vacuum at room temperature for 3 h and then weighed. The inorganic content of $AuSC_2Ph$ was 80%, as determined through the thermal gravimetric analyzer (TGA). Moreover, the pyridine-coated Au NPs (AuPy)

10.1021/ma0704764 CCC: $37.00
Published on Web 06/12/2007

Scheme 1. Fabrication of the Self-Assembled PS-*b*-P4VP/AuSC$_2$Ph Bulk Film

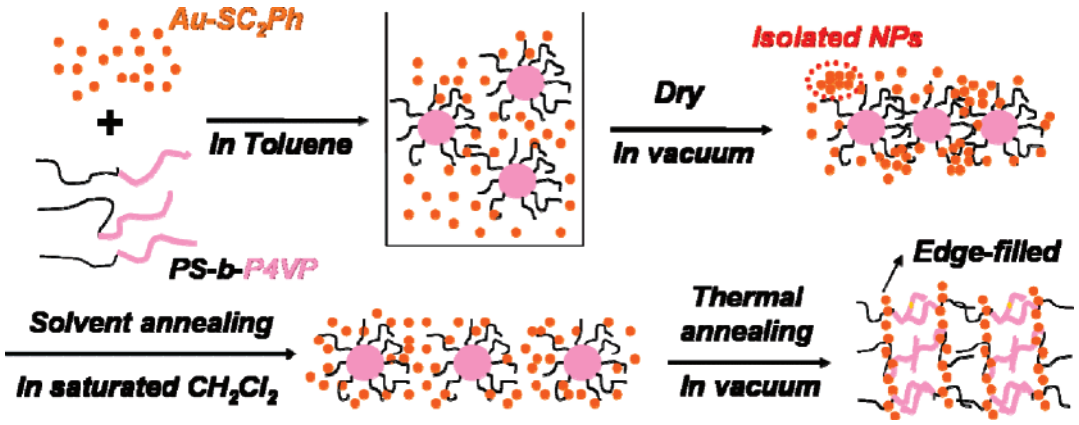

prepared to study the case of NP distribution throughout the P4VP domain were synthesized using a previously described method;[13] the volume loading of Au in the PS-*b*-P4VP$_{Sph}$/AuPy mixture was 1.4%.

Preparation of Block Copolymer/Au NP Mixtures. To study the edge-filled assembly, PS-*b*-P4VP/AuSC$_2$Ph was prepared as outlined in Scheme 1. PS-*b*-P4VP (30 mg) was added to toluene (1 mL). AuSC$_2$Ph NPs, having a volume fraction of Au of 1.4% in the PS-*b*-P4VP/AuSC$_2$Ph mixtures, were added to the micellar solution; to obtain a final solid concentration of 2 wt %, additional toluene was added. After stirring for 48 h, the toluene was evaporated slowly under vacuum at room temperature, and then the PS-*b*-P4VP/AuSC$_2$Ph solid film was dissolved in dichloromethane. The composites were mixed for 48 h and dried under a nitrogen flow until a saturated solution had formed. Subsequently, the mixtures were treated to a two-step annealing process involving annealing in saturated dichloromethane solution at 30 °C for 48 h, and drying slowly, followed by thermal annealing at 170 °C for 72 h to obtain the bulk PS-*b*-P4VP/AuSC$_2$Ph composites. The thin-film PS-*b*-P4VP/AuSC$_2$Ph was formed from a dilute micellar solution (0.5 wt %) that was prepared by dissolving annealed PS-*b*-P4VP/AuSC$_2$Ph in toluene. The PS-*b*-P4VP/AuPy composite, in which Au NPs were confined in P4VP spheres, were prepared as described previously.[13]

Characterization. Transmission electron microscopy was performed using a Hitachi H-600 instrument operated at 100 kV (for higher-contrast images) and a JEOL-2010 TEM operated at 200 kV (for higher-resolution and lattice images). For TEM studies, ultrathin slices of the bulk films of the PS-*b*-P4VP/AuSC$_2$Ph mixtures were microtomed using a Leica Ultracut Uct apparatus equipped with a diamond knife and then deposited onto copper grids. In the case of thin films, a 0.5 wt % PS-*b*-P4VP/AuSC$_2$Ph composite solution was mixed in toluene for 3 days, dropped directly onto the carbon-coated copper grids, and dried of its additional solvent using absorbent paper. Small-angle X-ray scattering (SAXS) measurements were performed at the SWAXS endstation of the BL17B3 beamline of the National Synchrotron Radiation Research Center (NSRRC). The flexible instrument was reported in details previously.[31,32] With a 0.5 mm diameter beam of a wavelength λ of 1.24 Å and a sample-to-detector distance of 2.4 m, we collected SAXS data in the Q range from 0.006 to 0.25 Å^{-1}, which Q range covered the scattering characteristics of Au nanoparticle and the large Au−copolymer complex. Here the wave vector transfer $Q = 4\pi \sin(\theta/2)/\lambda$ was defined by the scattering angle θ and wavelength λ of X-rays. Sample solutions in toluene were sealed (airtight) in a cell with thin Kapton windows and a sample thickness of 5.2 mm. All the SAXS data collected with an area detector were corrected for sample transmission, background, and the detector sensitivity, and the Q value was calibrated by a commonly used silver behenate. For SAXS sample preparation, the bulk films were ca. 20 μm in thickness; the composite solution was mixed for 3 days with a solid content of 0.5 wt % in toluene. X-ray photoelectron spectroscopy (XPS) experiments were performed using the wide-range spherical grating monochromator (WR-SGM) beamline at the BL24A1 beamline of the NSRRC and a mu-metal chamber equipped with a VG CLAM2 triple-channeltron energy analyzer (energy resolution was estimated to be better than 0.3 eV) and a sample transfer mechanism. The electron takeoff angle is 90°, and the incidence angle is 42°. All XPS samples that had been annealed and redissolved in dichloromethane were prepared by spin-coating onto low-resistance ITO substrates (ca. 10 Ω/□) followed by removal of the residual solvent under vacuum overnight.

Results and Discussion

Figure 1a displays the TEM micrograph of AuSC$_2$Ph NPs having a relatively uniform and narrow size distribution (diameter: 2.4 nm). Figure 1b indicates that the number-averaged particle diameter was 2.4 ± 0.1 nm, with a polydispersity of 15%, as deduced from the fitting of the SAXS data with a spherical form factor and a Schultz size distrubution.[12e] The TEM and SAXS results correspond quite well. Because the ligands on the as-prepared AuSC$_2$Ph NPs were hydrophobic (i.e., then presented phenyl groups), the AuSC$_2$Ph NPs had more affinity to the PS block than to the P4VP block after the solvent being removed.

Figure 2 indicates that the SAXS curve of pure PS-*b*-P4VP$_{Sph}$ in toluene can be fitted to a core/corona-like structure that consists of a P4VP domain as the core (diameter: 18 nm) and a PS domain as the corona (overall diameter: 36 nm). The polydispersity of the core/corona structure was 25%, due to the polydispersity of the molecular weight (PDI = 1.07) of PS-*b*-P4VP$_{Sph}$. The SAXS curve of the as-prepared mixture in toluene was approximated by the sum of the individual SAXS curves of PS-*b*-P4VP$_{Sph}$ in toluene and AuSC$_2$Ph in toluene, indicating that there were no interactions (no interference scattering) between PS-*b*-P4VP$_{Sph}$ and AuSC$_2$Ph in toluene, even after they had been mixed for 3 days. Presumably, AuSC$_2$Ph NPs prefer to stay in the toluene phase rather than adsorb to the PS corona or the P4VP core in the solution state.

Figure 3a displays the SAXS curves of the in situ annealed bulk PS-*b*-P4VP$_{Sph}$/AuSC$_2$Ph mixture that had previously experienced solvent annealing. The SAXS curves display two distinct changes: the absolute intensity underwent a dramatic increase in the low-Q range (between 0.03 and 0.08 Å^{-1}) and a large decrease in the high-Q range (ca. 0.18 Å^{-1}). The increase of the scattering intensity can be divided into two stages: the early and later stages of the annealing process. In the early stage, the increase of intensity is attributed to the formation of stronger correlations between the Au NPs in the PS-*b*-P4VP. During this time, the Au NPs diffuse to the interfaces between the PS and P4VP, forming the Au NP-filled shell, which in turn results in

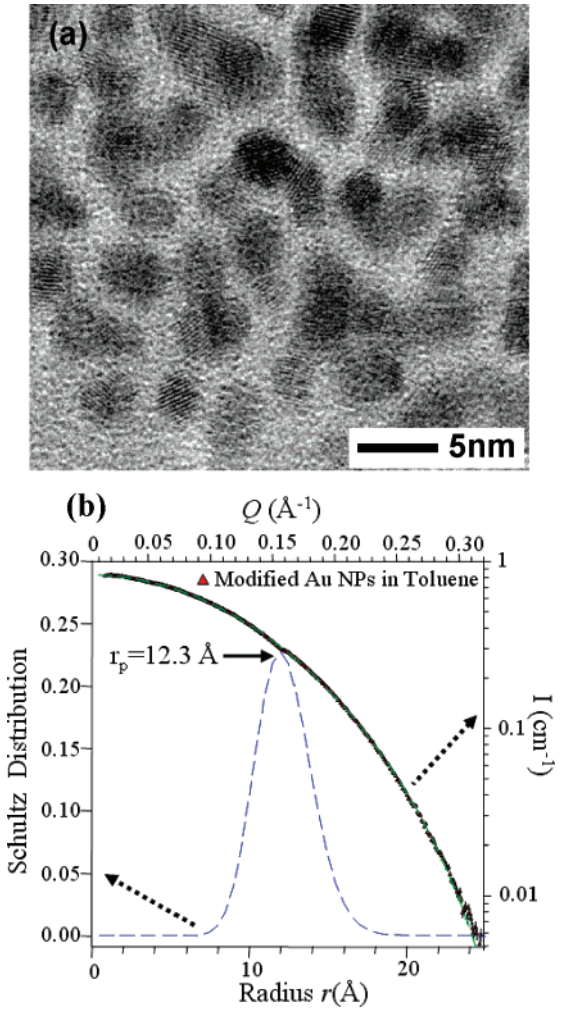

Figure 1. (a) HR-TEM image of $AuSC_2Ph$ cast from a toluene solution. (b) The SAXS profile measured for the 0.5 wt % $AuSC_2Ph$ NPs in toluene is fitted (dashed curve) using polydisperse spheres of the Schultz distribution (in radius *r*) shown.

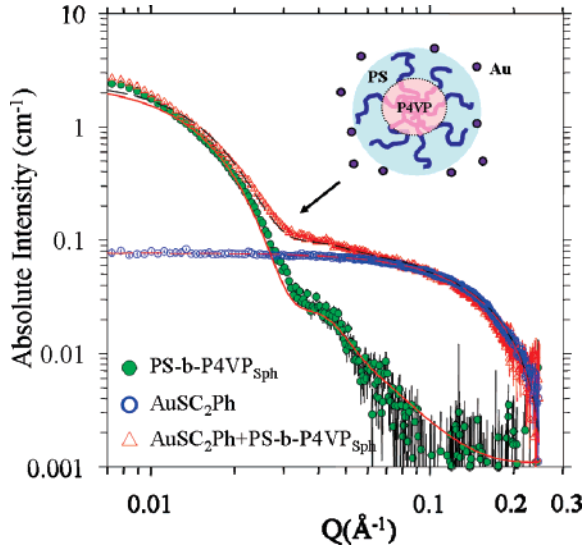

Figure 2. Solution SAXS profiles of the as-prepared PS-*b*-$P4VP_{Sph}$, $AuSC_2Ph$, and the PS-*b*-$P4VP_{Sph}$/$AuSC_2Ph$ mixture in toluene.

a stronger scattering intensity and more-ordered scattering peaks (the scattering peaks appear in the *Q* range between 0.03 and 0.08 $Å^{-1}$). It appears that the ordering of PS-*b*-$P4VP_{Sph}$ improved after simply raising the temperature to 170 °C. Figure 3b indicates, however, that the annealed pure PS-*b*-$P4VP_{Sph}$

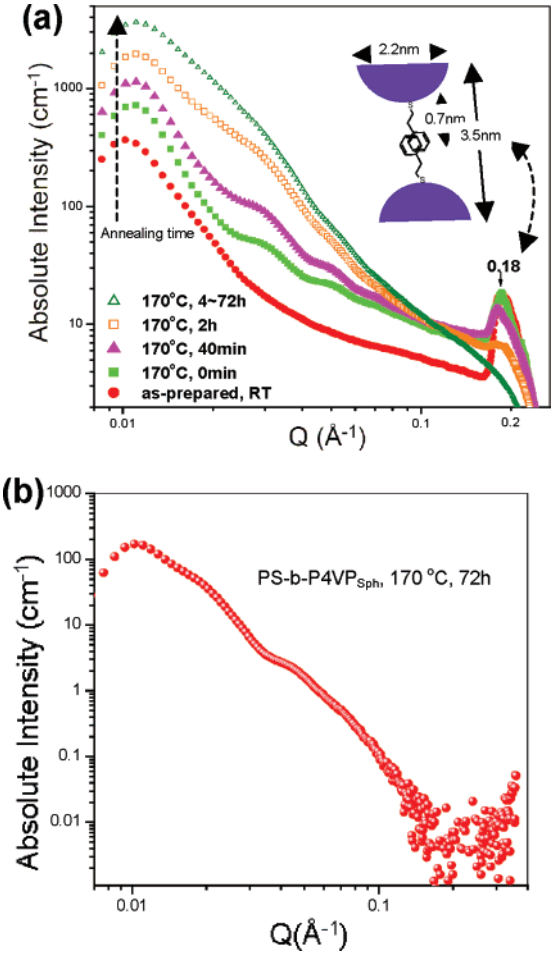

Figure 3. (a) In situ thermal annealing SAXS profiles of the as-prepared PS-*b*-$P4VP_{Sph}$/$AuSC_2Ph$ mixture. (b) The SAXS profile of the annealed PS-*b*-$P4VP_{Sph}$.

displayed different oscillations and a low absolute scattering intensity after annealing for 72 h. The morphology of pure PS-*b*-$P4VP_{Sph}$ bulk film was composed of disordered micelles because the scattering profile of the bulk film (Figure 3b), after scaled down in intensity, can overlap well with that for the micelles (Figure 2). From a comparison of the SAXS curves in Figure 3a,b, we deduce that the stronger oscillations of the mixture were dominated by the spatial distribution of Au NPs; namely, the coherent or constructive interference of the P4VP/Au complex contributes to the much higher intensity than that of the random dispersion or aggregation of Au NPs. In the second stage (annealing time: >1 h), the Au NPs appeared to accumulate in the interfacial area between the two blocks. A certain degree of overlapping or aggregation of the Au NPs occurred at PS/P4VP interfaces, which deteriorated the shell structure and the corresponding ordering of the peaks. Moreover, the scattering peak of the composite at a value of *Q* of ca. 0.18 $Å^{-1}$ suggests a liquidlike ordering of the Au NPs in the PS phase after the solvent had evaporated. It seems likely that, protected by their attached ligands (see the inset of Figure 3a), the Au NPs did not aggregate but instead packed into a liquidlike ordering phase (possibly because of the nature of the ligand of the soft chains) with a mean spacing ($2\pi/Q$) of 3.5 nm, corresponding quite well to the diameter of the Au NPs (2.2 nm) plus twice the length of the 2-phenylethanethiol ligand (2 × 0.7 nm = 1.4 nm). As a consequence, the correlated hierarchical structure increases the scattering intensity of the composite, at a cost of the phase-separated Au NP clusters (i.e., decreased intensity of the 0.18 $Å^{-1}$ peak). The peak of the Au

Scheme 2. Schematic Illustrations of the Structural Evolution of the PS-*b*-P4VP$_{Sph}$/AuSC$_2$Ph Mixture at Different Annealing Times

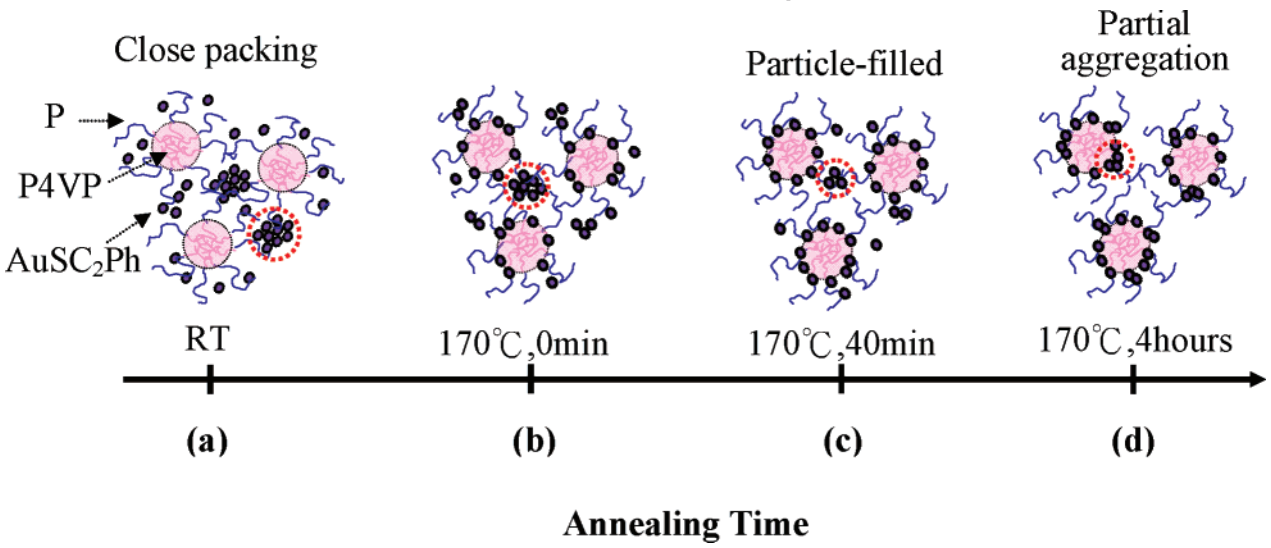

NP clusters at 0.18 Å^{-1} disappeared completely after 4 h of annealing and remained so even after increasing the annealing time, indicating that the structure transformation of the composite, closely associated with the Au NPs, did not change furthermore after the complete disruption of the Au NPs clusters in the first 4 h of the thermal annealing. Scheme 2 displays the schematic drawing of the structural evolution of PS-*b*-P4VP$_{Sph}$/AuSC$_2$Ph mixture during the thermal annealing. In Scheme 2, in the early stage of thermal annealing, the structure of the mixture is represented by Scheme 2a−c, whereas in the later stage, Scheme 2d stands for its structure.

In fact, the much higher scattering intensity in low-Q range after thermal annealing is a result of the complex formation of the copolymer and Au NPs. Namely, the formation of NP-filled complex or the adsorption of Au NPs to the copolymer. We also provided more evidence on the structural evolution of PS-*b*-P4VP$_{Sph}$/AuSC$_2$Ph mixture by using anomalous SAXS and TEM. Anomalous SAXS (Figure S1) is used to discern the scattering contribution of Au NPs.[31] To identify the scattering peak at $Q = 0.18$ Å^{-1}, the anomalous SAXS result for the PS-*b*-P4VP$_{Sph}$/AuSC$_2$Ph film was displayed in Figure S1a before the thermal annealing. With the X-ray energy tuned closed to the K-absorption edge of gold (11.919 keV), the SAXS profile is expected to be sensitive only to the distribution of Au NPs in the composite film due to the resonant absorption. The two SAXS profiles in Figure S1a was obtained with 11.200 and 11.910 keV (away and near the K-absorption edge of Au) photons. The two profiles overlap well in the low-Q region (insensitive to the energy change, see also the inset), indicating that the high scattering intensity in this region does not involve Au NPs and should be mainly dominated by the P4VP spheres of the copolymer. On the other hand, in the high-Q region (see also the inset), the scattering peak at $Q = 0.18$ Å^{-1} decreases obviously when the photon energy is changed from 11.200 to 11.910 keV. This result indicates clearly that the Au NPs, forming ordered clusters, are responsible for the ordering peak at $Q = 0.18$ Å^{-1}. Furthermore, the overall scattering SAXS profile for the mixture film after thermal annealing in Figure S1b is sensitive to the beam energy close to the K-edge absorption of Au. This illustrates that the overall scattering profile including the low-Q region dominated by the pure PS-*b*-P4VP$_{Sph}$ before thermal annealing closely associates with Au NPs after the thermal annealing. From anomalous SAXS data of PS-*b*-P4VP$_{Sph}$/AuSC$_2$Ph mixtures before and after thermal annealing, it is clear that Au NPs adsorb to the PS/P4VP interface only after thermal annealing. Figure 4 shows TEM images of PS-*b*-P4VP$_{Sph}$/AuSC$_2$Ph mixtures before and after thermal annealing. Figure 4a displays TEM image of the as-prepared PS-*b*-P4VP$_{Sph}$/AuSC$_2$Ph mixture. We can observe few Au NP clusters, which agree with the in situ SAXS result in Figure 3a and the drawing in Scheme 2a. Figure 4b displays the TEM image of PS-*b*-P4VP$_{Sph}$/AuSC$_2$Ph mixture that experienced the two-step solvent and thermal annealing. Because of the slice thickness of the bulk spherical diblock copolymer, overlapped spheres are visible in this TEM image. In the inset in Figure 4b, an HR-TEM cross-sectional image of a single P4VP/AuSC$_2$Ph core−shell sphere, we observe the formation of an Au NP-filled shell, quite consistent with the SAXS results of the in situ bulk thermal annealing. Hence, the evidence from these TEM images supports the conclusion from in situ SAXS results. From all the evidence mentioned above, we are confident on the conclusion given in Scheme 2 for the structural evolution of PS-*b*-P4VP$_{Sph}$/AuSC$_2$Ph mixtures during thermal annealing process.

Since the thermal annealing process will result in a loss of thiol ligands on the surface of Au NPs, we quantified the loss of 2-phenylethanethiol by TGA. Figure 5a shows the weight loss curve of the PS-*b*-P4VP$_{Sph}$/AuSC$_2$Ph during the thermal annealing. The additional weight loss of the PS-*b*-P4VP$_{Sph}$/AuSC$_2$Ph mixture between before and after thermal annealing is 1.2 wt % at 230 °C (2-phenylethanethiol ligands of AuSC$_2$-Ph will evaporate off at 230 °C), which is equal to a 68.6% loss of 2-phenylethanethiol ligands (1.75 wt %, initially). The partial loss of the hydrophobic thiol ligands on Au NPs' surfaces was compensated by having been surrounded by the pyridine groups of P4VP chains when Au NPs diffused to the PS/P4VP interface. To monitor the weight loss of thiol ligands, the PS-*b*-P4VP/AuSC$_2$Ph mixture was annealed in TGA furnace at 170 °C under a N_2 atmosphere. Figure 5b shows the weight loss vs the annealing time with a deep loss of thiol ligands in the first hour of thermal annealing. The weight loss of 0.7 wt % of the composite corresponds to a 40% loss of the thiol ligands. The TGA results provide the evidence that some of the 2-phenylethanethiol ligands have evaporated during the thermal annealing, leading to a decrease in the hydrophobicity and the thiol grafting density of AuSC$_2$Ph NPs.

Figure 6 displays the results of SAXS for the annealed PS-*b*-P4VP$_{Sph}$/Au NP mixture redissolved in toluene. In Figure 6a,

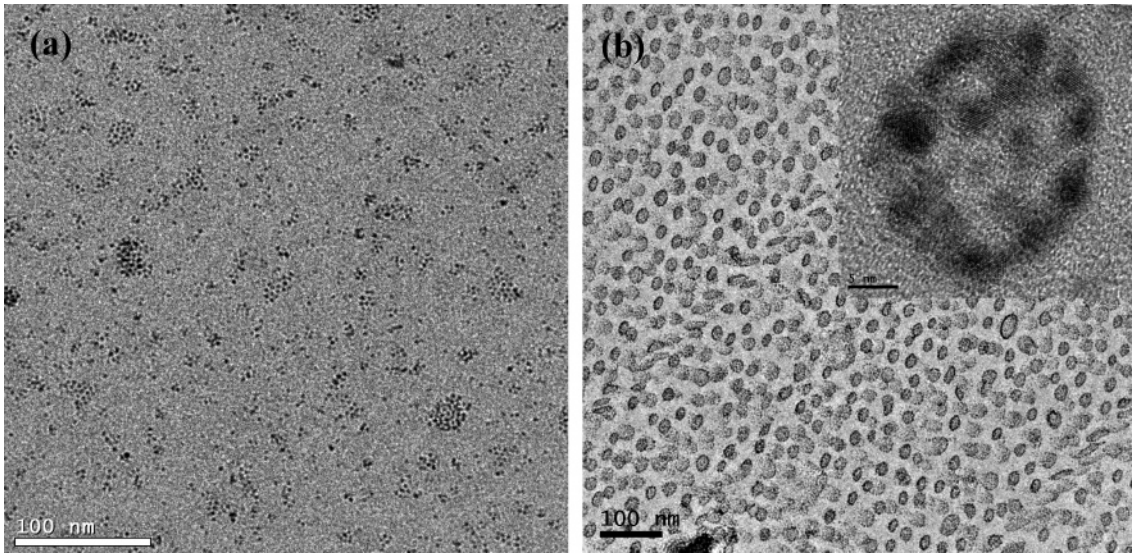

Figure 4. (a) TEM image for the as-prepared PS-b-P4VP$_{Sph}$/AuSC$_2$Ph mixture, with abundant NP clusters. (b) TEM micrograph of the PS-*b*-P4VP$_{Sph}$/AuSC$_2$Ph mixture that had been subjected to two-step annealing, 48 h of solvent annealing at 30 °C, and 72 h for thermal annealing at 170 °C. Inset: HR-TEM image of a single P4VP$_{Sph}$/AuSC$_2$Ph core/shell assembly.

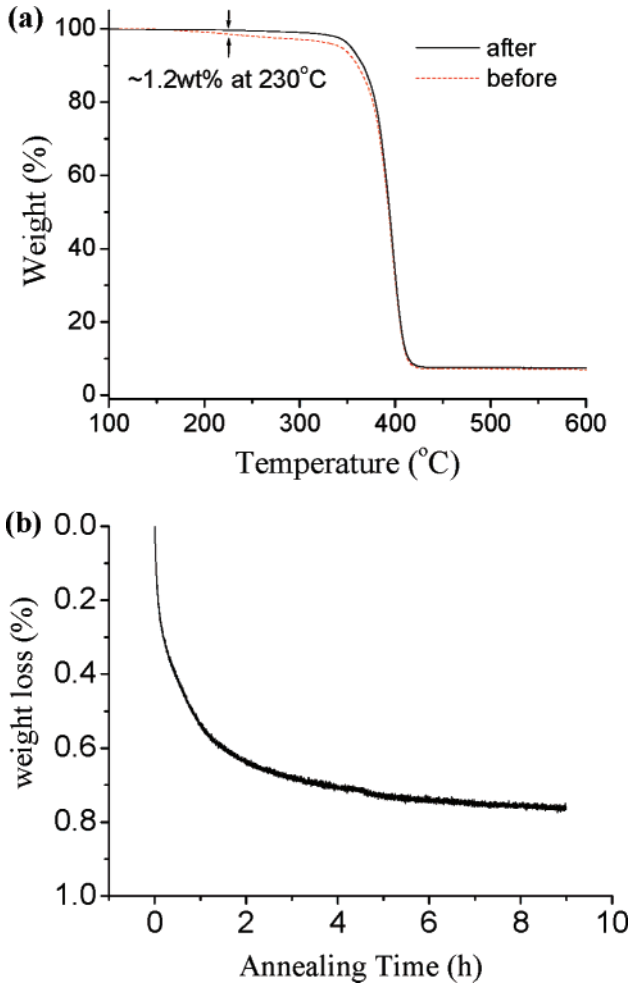

Figure 5. (a) TGA result of the PS-*b*-P4VP$_{Sph}$/AuSC$_2$Ph mixture before and after 72 h thermal annealing at 170 °C under vacuum. (b) The weight loss (%) vs the annealing time of the PS-*b*-P4VP$_{Sph}$/AuSC$_2$Ph mixture during the 170 °C isothermal annealing under a N_2 atmosphere.

the SAXS curve for the solution of PS-*b*-P4VP$_{Sph}$/AuSC$_2$Ph exhibits stronger oscillation characteristics, reflecting a higher hierarchical structural order for the mixture, than that for pure PS-*b*-P4VP$_{Sph}$, in toluene solution. The higher electron density at the interface can be used to fit the curves (dashed curve), implying that the Au NPs reside at the interface between the PS and P4VP blocks. Additionally, the Au NPs remained well dispersed at the interface, as evidenced from the high-Q region of the same transition feature, which is the same as that of the pure Au NPs having a diameter of 2.2 nm. In contrast, in the case of the PS-*b*-P4VP$_{Sph}$/AuPy solution,[13] the SAXS scattering characteristics revealed that the Au NPs were incorporated within the P4VP domain, forming aggregates having an average diameter of 5 nm. In Figure 6b, the three plots of the ln $I(Q)$ vs Q^2 data were fitted using the corresponding Guinier approximations (dashed lines) in the low-Q range of 0.006−0.012 Å^{-1}, as represented by eq 1:

$$I(Q) = I(0)\exp\left(-\frac{Q^2R_g^2}{3}\right) \quad (1)$$

where R_g is the radius of gyration of the diblock copolymer in solution and can be extracted from the slopes ($-R_g^2/3$) of the fitted lines in Figure 6b. The values of R_g for the PS-*b*-P4VP$_{Sph}$, PS-*b*-P4VP$_{Sph}$/AuSC$_2$Ph, and PS-*b*-P4VP$_{Sph}$/AuPy systems were 148 ± 5, 152 ± 3, and 173 ± 5 Å, respectively. Thus, when the Au NPs were incorporated within the P4VP domains, the global size of the composite increased to 173 from 148 Å for the pure PS-*b*-P4VP$_{Sph}$. This result can be understood by considering the fact that the P4VP chains are tangled with Au NPs and, therefore, are stretched to accommodate neighboring Au NPs. In contrast, when the Au NPs were bound at the interface between the PS and P4VP blocks, the global size was virtually identical to that of the pure block copolymer. Presumably, the Au NPs at the interface of the PS and P4VP blocks reside in the corona-like chains of PS, which remained in an extended state in toluene, a favorable solvent for PS. Therefore, the PS-*b*-P4VP$_{Sph}$/AuSC$_2$Ph system formed a core/shell/corona (P4VP/Au/PS) micellar structure.

Figure 7 displays TEM images of a PS-*b*-P4VP$_{Sph}$/AuSC$_2$Ph thin film that had been cast from the solution of two-step annealed PS-*b*-P4VP$_{Sph}$/AuSC$_2$Ph mixture in toluene. In Figure 7a, it is notable that the NP-filled shell nanopatterns remained despite the fact that they have undergone the recasting. Moreover, the TEM image of a single P4VP/AuSC$_2$Ph core/shell structure in Figure 7b indicates less deformed P4VP

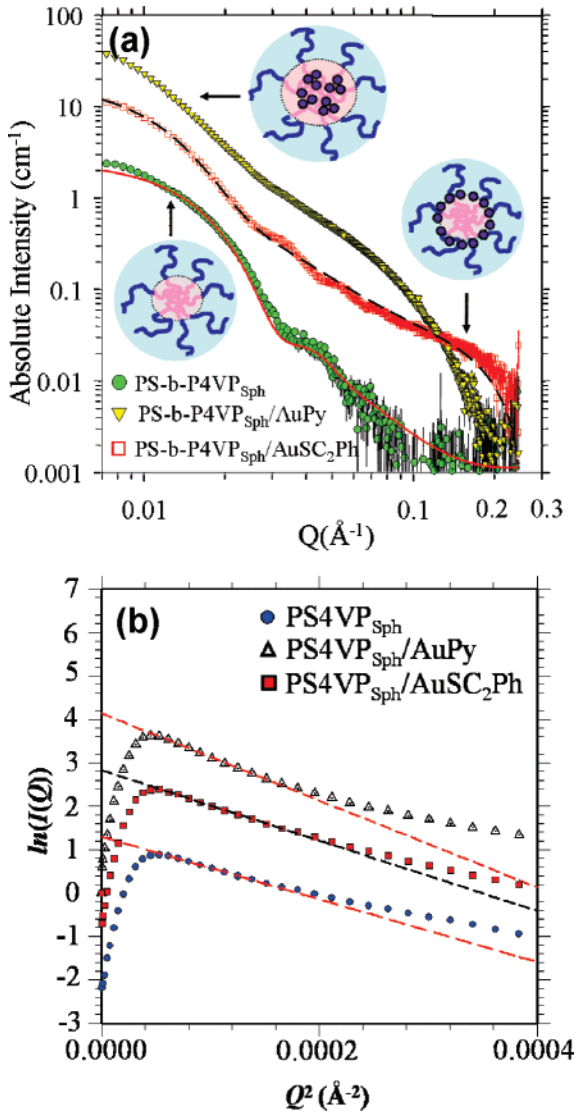

Figure 6. (a) Solution state SAXS profiles of the PS-*b*-P4VP$_{Sph}$, PS-*b*-P4VP$_{Sph}$/AuPy, and PS-*b*-P4VP$_{Sph}$/AuSC$_2$Ph systems after they had been subjected to annealing and redissolving in toluene. All schematic micellar structures of PS-*b*-P4VP$_{Sph}$−Au NP mixtures appear near the corresponding curves. (b) Three corresponding profiles fitted using the Guinier approximation.

spheres than that in the case of the bulk sample (Figure 4b); this result is probably due to the fact that the shear strain of the bulk from microtoming was released in the solution. On the basis of the volume fractions and diameters of the Au NP and P4VP spheres, we calculate that there were ca. 66 Au NPs locating at the interface of PS/P4VP domains, which amounts to a covered surface area of 24.7% for each P4VP sphere of the Au particle-filled nanoshell assembly (see Supporting Information); this result agrees quite well with the TEM observations in Figure 7b (ca. 60−80 Au NPs surrounding each P4VP sphere).

Overall, the irreversible structure after annealing and the stable nanoshell arrangement of Au NPs in bulk state and the redissolved micellar solution state imply that an additional chemical affinity may be generated between the 2-phenylethanethiol-coated Au NPs and the P4VP block in the thermal annealing process.

Figure 8 presents scanning XPS spectra of the pure P4VP, the annealed P4VP/AuSC$_2$Ph composites, the annealed lamellar PS-*b*-P4VP/AuSC$_2$Ph composites, and the as-prepared AuSC$_2$-Ph NPs. We attribute the peaks at 400, 286, 164, 153, 103, 88, and 84 eV to the N 1s (P4VP), C 1s, S 2p$_{3/2}$ (2-phenylethanethiol), Si 2s, Si 2p$_{3/2}$ (ITO), Au 4f$_{7/2}$, and Au 4f$_{5/2}$ (Au NPs) energy levels, respectively. Figure 9 displays the N 1s high-resolution XPS spectra of the pure P4VP, the annealed P4VP/AuSC$_2$Ph composite, and the annealed lamellar PS-*b*-P4VP/AuSC$_2$Ph composite. The N 1s signal of the pure P4VP presented a peak at 399.3 eV; the annealed P4VP/AuSC$_2$Ph and lamellar PS-*b*-P4VP/AuSC$_2$Ph composites exhibited higher binding energies, with their peaks at 400.1 and 399.8 eV, respectively. This slight increase is indicative of the interaction between the pyridine groups and the metallic Au NP surfaces. In fact, in the similar case of a poly(2-vinylpyridine)/Au NP system,[25,34] Shull et al. reported evidence for a strong Au−pyridine interaction by measuring a low contact angle (9°) between the Au and poly(2-vinylpyridine) surfaces. As a result, we surmise that the thermal annealing process caused the loss of the 2-phenylethanethiol ligands on the Au NP surfaces, resulting in enthalpic adsorption between the Au surfaces and the pyridine groups.

In addition to the entropic effect, the extra strong favorable interaction between P4VP or PS and Au NP surfaces determines the Au NPs location. Here, we only show the latter term quantitatively. The presence of stable NP-filled assemblies both in the bulk and in micellar solution can be partly explained by the interfacial adsorption energy of the NPs when they are located at the interface of the two phases. The adsorption energy (E_a) of an Au NP at the interface of PS-*b*-P4VP$_{Sph}$ in our experiments can be described using the following equation:[24,33]

$$E_a = \pi r^2 \gamma_{PS/P4VP}[1 - |\cos\theta|]^2 \quad (2)$$

where cos θ can be written as

$$\cos\theta = \frac{\gamma_{Au/PS} - \gamma_{Au/P4VP}}{\gamma_{PS/P4VP}} \quad (3)$$

where r is the radius of AuSC$_2$Ph and $\gamma_{PS/P4VP}$, $\gamma_{Au/P4VP}$, and $\gamma_{Au/PS}$ are the interfacial energies of the PS−P4VP diblock, the AuSC$_2$Ph−PS, and AuSC$_2$Ph−P4VP systems, respectively. In the annealed samples, the loss of phenylethanethiolate ligands (PS affinity surfaces) generated bare Au surfaces (P4VP affinity surfaces), leading to amphiphilic surfaces on the Au NPs. This situation will result in a slight difference between $\gamma_{Au/P4VP}$ and $\gamma_{Au/PS}$, approximated as zero for cos θ, giving a value of E_a of ca. $\pi r^2\gamma_{PS/P4VP}$ for an Au NP. Consequently, the adsorption energy contributed by the favorable interaction between P4VP and Au NPs may yield a driving interfacial assembly of NPs, not accounting for entropic considerations. Additionally, in the liquid phase, a recent report described the formation of macroscale NP-filled hollow spherical shells at liquid−liquid (toluene−water) interfaces.[35] In the case of our micellar solution, the P4VP−Au−PS core/shell/corona micellar solution in toluene would be stabilized as a result of the strong interactions (E_a = ca. $\pi r^2\gamma_{PS/P4VP}$) between Au and vinylpyridine, despite the fact that $\gamma_{Au/PS}$ replaces $\gamma_{Au/toluene}$. Therefore, the interfacial adsorption energy plays an important role on stabilizing the Au NP-filled assemblies in the micellar solution status.

We have shown that the location of the Au NPs can be altered by the evaporation of 2-phenylethanethiol ligands, which has a similar but short chemical structure to PS oligomer, during the thermal annealing process. In a related study, Kim et al. also demonstrated a similar mechanism to control the location of thiol-terminated PS or P2VP-coated Au NPs in a lamellar phase of P2-*b*-P2VP by directly synthesizing different grafting densities of thiol-terminated homopolymer on Au NPs.[25] For example,

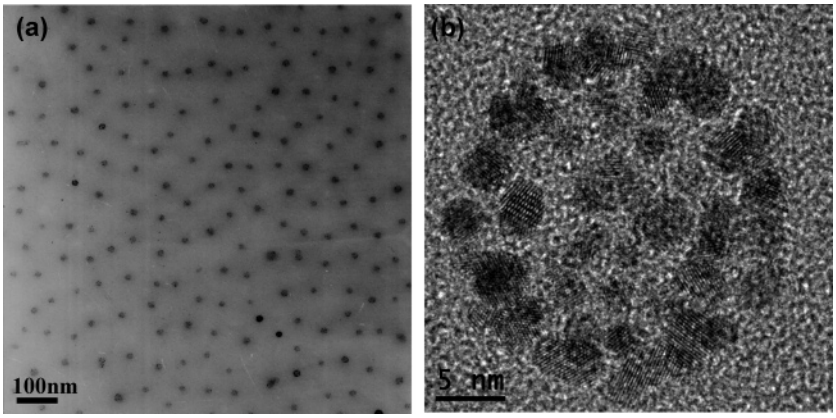

Figure 7. (a) TEM image of a recast thin film of the PS-*b*-P4VP$_{Sph}$/AuSC$_2$Ph mixture that had been subjected to annealing. (b) HR-TEM image of a single P4VP$_{Sph}$/AuSC$_2$Ph core/shell assembly.

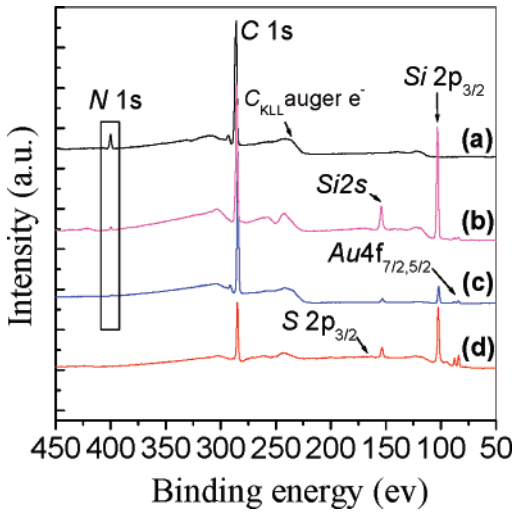

Figure 8. Survey scanning XPS spectra of the pure P4VP (a), the annealed P4VP/AuSC$_2$Ph composites (b), the annealed lamellar PS-*b*-P4VP/AuSC$_2$Ph composites (c), and the as-prepared AuSC$_2$Ph NPs (d). The edge-filled lamellar case has much higher N atom concentration (5 times for spherical case) for a better observation.

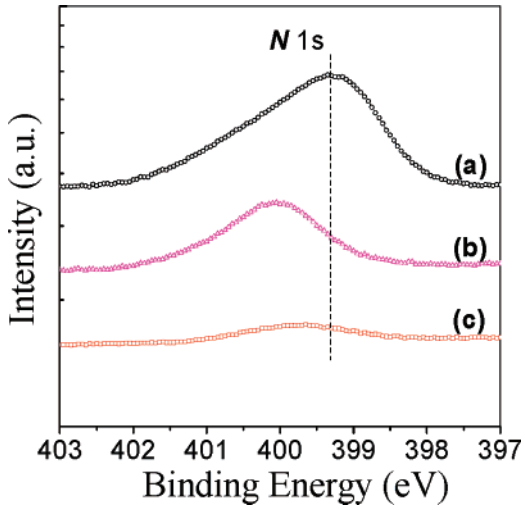

Figure 9. N 1s XPS spectra of the pure P4VP (a), the annealed P4VP/AuSC$_2$Ph composites (b), and the annealed lamellar PS-*b*-P4VP/AuSC$_2$-Ph composites (c).

high area chain density (>1.6 chains/nm^2) of PS-coated Au NPs can locate in the PS domain, whereas low area chain density ones (<1.3 chains/nm^2) can be incorporated into the PS/P2VP interface. In our case, we chose 2-phenylethanethiol as the ligand to fully cover the Au NPs, and we can obtain AuSC$_2$Ph NPs with a narrow size distribution of 15% and a good dispersion of the NPs in toluene solution. Owing to the small molecular ligands, the ligand cover density (or the location) of the Au NPs we used could be changed by the thermal annealing process, and the partial grafting Au NPs could stably embedded into the copolymer. Both systems are very similar in that the location of NPs can be influenced greatly by the chemical structure and the grafting density of the ligands on the NP surfaces via simple synthesis or annealing methods.

In summary, we have monitored the structural evolution of spherical PS-*b*-P4VP/AuSC$_2$Ph NP mixtures in the solid state during thermal annealing. We found that the Au NPs that existed in a random state with some cluster packing in the PS domain diffused to the interface of the amphiphilic PS-*b*-P4VP diblock copolymer within 4 h at 170 °C under vacuum to form NP-filled shell-like assemblies. We speculate that this interfacial activity of AuSC$_2$Ph results most from the fact that the initially hydrophobic Au NP surfaces became more hydrophilic after ~70% of the 2-phenylethanethiol ligands had evaporated off. The Au NP-filled assemblies located at the interface between the PS and P4VP blocks were quite stable; they remained in the form of PS−Au−P4VP core/shell/corona onion micelles even after redissolving the samples in toluene.

Acknowledgment. We thank the National Science Council, Taiwan, for funding (NSC 95-2120-M-009-012) and the National Synchrotron Radiation Research Center, Taiwan, for analytical support. We thank Dr. Ying-Huang Lai of National Synchrotron Radiation Research Center, Taiwan, for his help with SAXS measurement.

References and Notes

(1) Förster, S.; Antonietti, M. *Adv. Mater.* **1998**, *10*, 195−217.
(2) Bockstaller, M. R.; Mickiewocz, R. A.; Thomas, E. L. *Adv. Mater.* **2005**, *17*, 1331−1349.
(3) Shenhar, B. R.; Norsten, T. B.; Rotello, V. M. *Adv. Mater.* **2005**, *17*, 657−669.
(4) Haryono, A.; Binder, W. H. *Small* **2006**, *2*, 600−611.
(5) Balazs, A. C.; Emrick, T.; Russell, T. P. *Science* **2006**, *314*, 1107−1110.
(6) Fink, Y.; Urbas, A. M.; Bawendi, M. G.; Joannopoulos, J. D.; Thomas, E. L. *J. Lightwave Technol.* **1999**, *17*, 1963−1969.
(7) Lopes, W. A.; Jaeger, H. M. *Nature (London)* **2001**, *414*, 735−738.
(8) Li, C. P.; Wei, K. H.; Huang, J. Y. *Angew. Chem., Int. Ed.* **2006**, *45*, 1449−1453.
(9) Li, C. P.; Wu, C. H.; Wei, K. H.; Sheu, J. T.; Huang, J. Y.; Liang, K. S.; Jeng, U. S. *Adv. Funct. Mater.*, in press.
(10) Naito, K.; Hieda, H.; Sakurai, M.; Kamata, Y.; Asakawa, K. *IEEE Trans. Magn.* **2002**, *38*, 1949−1951.
(11) (a) Spatz, J. P.; Roescher, A.; Sheiko, S.; Krausch, G.; Moller, M. *Adv. Mater.* **1995**, *7*, 731−735. (b) Tsutsumi, K.; Funaki, Y.; Funaki, Y.; Hirokawa, Y.; Hashimoto, T. *Langmuir* **1999**, *15*, 5200−5203.

(c) Sohn, B. H.; Seo, B. H.; Seo, B. W.; Yun, S. H.; Park, S. M. *J. Am. Chem. Soc.* **2001**, *123*, 12734−12735.
(12) (a) Hamdoun, B.; Ausserre, D.; Joly, S.; Gallot, Y.; Cabuil, V.; Clinard, C. *J. Phys. IV* **1996**, *6*, 493−501. (b) Yeh, S. W.; Wei, K. H.; Sun, Y. S.; Jeng, U. S.; Liang, K. S. *Macromolecules* **2003**, *36*, 7903−7907. (c) Weng, C. C.; Wei, K. H. *Chem. Mater.* **2003**, *15*, 2936−2941. (d) Sohn, B. H.; Choi, J. M.; Yoo, S. I.; Yun, S. H.; Zin, W. C.; Jung, J. C.; Kanehara, M.; Hirata, T.; Teranishi, T. *J. Am. Chem. Soc.* **2003**, *125*, 6368−6369. (e) Yeh, S. W.; Wei, K. H.; Sun, Y. S.; Jeng, U. S.; Liang, K. S. *Macromolecules* **2005**, *38*, 6559−6566. (f) Kim, B. J.; Chiu, J. J.; Yi, G. R.; Pine, D. J.; Kramer, E. J. *Adv. Mater.* **2005**, *17*, 2618−2622.
(13) (a) Thurn-Albrecht, T.; Schotter, J.; Kastle, G. A.; Emley, N.; Shibauchi, T.; Krusin-Elbaum, L.; Guarini, K.; Black, C. T.; Tuominen, M. T.; Russell, T. P. *Science* **2000**, *290*, 2126−2129. (b) Zhang, Q.; Xu, T.; Butterfield, D.; Misner, M. J.; Ryu, D. Y.; Emrick, T.; Russell, T. P. *Nano Lett.* **2005**, *5*, 357−361.
(14) Boal, A. K.; Iihan, F.; DeRouchey, J. E.; Thurn-Albrecht, T.; Russell, T. P.; Rotello, V. M. *Nature (London)* **2000**, *404*, 746−748.
(15) Buxton, G. A.; Lee, J. Y.; Balazs, A. C. *Macromolecules* **2003**, *36*, 9631−9637.
(16) Bockstaller, M. R.; Thomas, E. L. *Phys. Rev. Lett.* **2004**, *93*, 166106.
(17) Lin, Y.; Boker, A.; He, J. B.; Sill, K.; Xiang, H. Q.; Abetz, C.; Li, X. F.; Wang, J.; Emrick, T.; Long, S.; Wang, Q.; Balazs, A. C.; Russell, T. P. *Nature (London)* **2005**, *434*, 55−59.
(18) Thompson, R. B.; Ginzburg, V. V.; Matsen, M. W.; Balazs, A. C. *Science* **2001**, *292*, 2469−2472.
(19) Lee, J. Y.; Thompson, R. B.; Jasnow, D.; Balazs, A. C. *Macromolecules* **2002**, *35*, 4855−4858.
(20) Thompson, R. B.; Ginzburg, V. V.; Matsen, M. W.; Balazs, A. C. *Macromolecules* **2002**, *35*, 1060−1071.
(21) Lee, J. Y.; Thompson, R. B.; Jasnow, D.; Balazs, A. C. *Phys. Rev. Lett.* **2002**, *89*, 155503.
(22) Kim, J. U.; O'Shaughnessy, B. *Phys. Rev. Lett.* **2002**, *89*, 238301.
(23) Bockstaller, M. R.; Lapetnikov, Y.; Margel, S.; Thomas, E. L. *J. Am. Chem. Soc.* **2003**, *125*, 5276−5277.
(24) (a) Chiu, J. J.; Kim, B. J.; Kramer, E. J.; Pine, D. J. *J. Am. Chem. Soc.* **2005**, *127*, 5036−5037. (b) Sides, S. W.; Kim, B. J.; Kramer, E. J.; Fredrickson, G. H. *Phys. Rev. Lett.* **2006**, *96*, 250601.
(25) Kim, B. J.; Bang, J.; Hawker, C. J.; Kramer, E. J. *Macromolecules* **2006**, *39*, 4108−4114.
(26) Zubarev, E. R.; Xu, J.; Sayyad, A.; Gibson, J. D. *J. Am. Chem. Soc.* **2006**, *128*, 15098−15099.
(27) Spontak, R. J.; Shankar, R.; Bowman, M. K.; Krishnan, A. S.; Hamersky, M. W.; Samseth, J.; Bockstaller, M. R.; Rasmussen, K. Ø. *Nano Lett.* **2006**, *6*, 2115−2120.
(28) Listak, J.; Bockstaller, M. R. *Macromolecules* **2006**, *39*, 5820−5825.
(29) Brust, M.; Walker, M.; Bethell, D.; Schiffrin, D. J.; Whyman, R. *J. Chem. Soc., Chem. Commun.* **1994**, 801−802.
(30) Donkers, R. L.; Lee, D.; Murray, W. R. *Langmuir* **2004**, *20*, 1945−1952.
(31) Lai, Y. H.; Sun, Y. S.; Jeng, U. S.; Lin, J. M.; Lin, T. L.; Sheu, H. S.; Chuang, W. T.; Huang, Y. S.; Hsu, C. H.; Lee, M. T.; Lee, H. Y.; Liang, K. S.; Gabriel, A.; Koch, Michel, H. J. *J. Appl. Crystallogr.* **2006**, *39*, 871−877.
(32) Sun, Y. S.; Jeng, U. S.; Liang, K. S.; Yeh, S. W.; Wei, K. H. *Polymer* **2006**, *47*, 1101−1107.
(33) Pieranski, P. *Phys. Rev. Lett.* **1980**, *45*, 569−572.
(34) Kunz, M. S.; Shull, K. R.; Kellock, A. J. *J. Colloid Interface Sci.* **1993**, *156*, 240−249.
(35) (a) Lin, Y.; Skaff, H.; Emrick, T.; Dinsmore, A. D.; Russell, T. P. *Science* **2003**, *299*, 226−229. (b) Lin, Y.; Skaff, H.; Böker, A.; Dinsmore, A. D.; Emrick, T.; Russell, T. P. *J. Am. Chem. Soc.* **2003**, *125*, 12690−12691.

MA0704764